

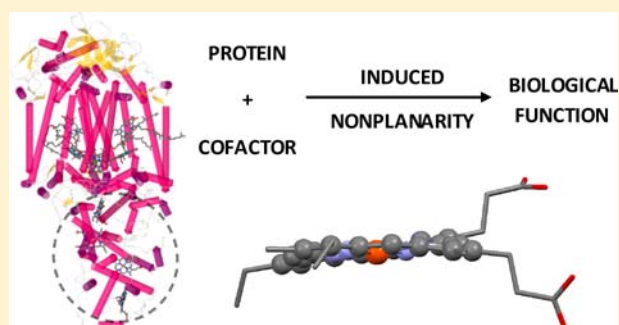
Computational Quantification of the Physicochemical Effects of Heme Distortion: Redox Control in the Reaction Center Cytochrome Subunit of *Blastochloris viridis*

Stuart A. MacGowan and Mathias O. Senge*

School of Chemistry, SFI Tetrapyrrole Laboratory, Trinity Biomedical Sciences Institute, 152-160 Pearse Street, Trinity College Dublin, Dublin 2, Ireland

S Supporting Information

ABSTRACT: A facile, experimentally calibrated computational procedure is described that affords the relative ordering of heme cofactor reduction potentials with respect to intrinsic shifts brought about by apoprotein induced heme-macrocycle distortion. The method utilizes heme-Fe partial atomic charges and is useful with the computationally inexpensive B3LYP/3-21g method calculated for simplified heme models extracted from the Protein Data Bank incorporating only the effects of varying macrocycle conformations and thereby delineating their physicochemical effects. The procedure was successfully calibrated using the atomic coordinates and published midpoint potentials from the heme cofactors in wild-type and a series of heme-NO and -O₂ binding domain mutants and thus confirmed the sole conformational modulation of the redox potentials in these complexes. This technique was also applied to the reaction center tetraheme cytochrome subunit of *Blastochloris viridis* to build upon previous work elucidating the role that conformational control plays in photosynthetic systems, and it was found that this effect may account for up to 70% (54mV) of the observed differences in the reduction potentials of the four hemes. We validate the approach using larger basis sets up to and including the triple- ζ , doubly polarized and augmented 6-311+g** basis and discuss the specific conformational origins of the effect.



INTRODUCTION

Hemeproteins and other tetrapyrrole containing biomolecules are one of the most diverse classes of enzymes present in the natural world.^{1–4} Through recognition of the homologies of the active constituents of the globins, cytochromes, and peroxidases (heme) as well as reaction centers and light-harvesting complexes (chlorophylls, bacteriochlorophylls, pheophytins) it is apparent that nature has evolved methods with which to utilize the same chemical cofactor for a range of disparate chemistries and enzymatic transformations, including electron transfer, small ligand binding, charge-separation, and exciton transfer.^{3,5,6} The plasticity of these cofactors with respect to physicochemical modulation in complexes is particularly emphasized by heme protein reduction potentials, which exhibit an impressive range spanning 1 V from –550 mV to +450 mV versus SHE⁷ and are a key-determinant of their biological functions.⁸ As an addition to the classical concepts of apoprotein cofactor control via axial ligation, H-bonding, and charged-residue electrostatic influences,^{1,8,9} we have advocated the structural importance of the conformational flexibility of the porphyrin macrocycle as a modulator of cofactor properties and function.¹⁰ Here, we build upon this work by assessing the role of conformational control in modulating the reduction potentials of the hemes in the reaction center tetraheme cytochrome subunit of *Blastochloris viridis* (RC-CYT) through

a combined statistical analysis of the heme conformations afforded by the available crystal structure data and subsequent application of an experimentally calibrated computational procedure.

Originally, the concept of conformational control arose from observations that the extended aromatic π -system of porphyrins was flexible with respect to distortion from planarity in structural studies on both synthetic and biological compounds that revealed the characteristic saddled, ruffled, and domed macrocycle conformations.^{11–14} The biological relevance of these observations was realized later when it was discovered that specific conformations were often conserved within particular enzyme classes.^{15–18} This, considered with the knowledge that the distortions were found to alter (often systematically) chromophore absorption, redox and excited state behaviors,^{12,19} provided an additional chemical rationale for the biological versatility of tetrapyrrole cofactors.

These physicochemical consequences of nonplanarity were deduced primarily from model compound studies which correlated increasing macrocycle distortion with bathochromic shifts of the UV/vis Q-bands, easier oxidation, and hindered reduction (for macrocycle centered redox processes) and

Received: July 13, 2012

Published: January 15, 2013

decreasing S_1 -lifetimes.^{12,19,20} In contrast however, computational investigations of macrocycle nonplanarity experienced a period of inconsistency, sparking lively debate among experts and giving rise to such controversies as the publicized debunking of nonplanar physicochemical modulation in favor of the short-lived concept of In-Plane Nuclear Rearrangement.^{21–24} This debate continued until specific flaws were identified in the structural models used, and it was once again widely accepted that it is the distortions of the porphyrinoid macrocycle that give rise to these effects.²² Considering this historical development, an experimentally verifiable computational method for evaluating the physicochemical effects of macrocycle structural perturbation is a desirable goal which has not yet been fully realized.

In this later respect, our approach was enabled by the recent work of Olea et al. where conformational control was used to impart redox modification through mutagenesis of the heme-NO and -O₂ binding domain (H-NO_x) from *Thermoanaerobacter tengcongensis*.²⁵ They reported that the reduction potential of the H-NO_x complex could be reduced via site-specific mutations that allowed the highly distorted heme cofactor to relax into a less nonplanar conformation. They also found that the decreased potentials were due to a measurable decrease of electron density at the heme-Fe as indicated by UV/vis spectroscopy and the pK_a 's of the bound aqua ligands. Since this study controlled for any nonconformational influences by selecting residue substitutions that changed neither the H-bonding of the cofactor nor the local dielectric environment, it presented an ideal reference from which to establish a quantitative relationship between the macrocycle conformation and distortion induced potential shifts through calculable quantum mechanical properties of the isolated hemes.

With this relationship in hand, we continued our work regarding nature's exploitation of conformational control to enhance the efficiency of photosynthetic reaction centers and decided to assess the role macrocycle distortion plays in the modulation of the redox potentials of the individual hemes in the reaction center tetraheme cytochrome subunit of *B. viridis* (RC-CYT). This subunit is tethered to the reaction center in the periplasmic space above the membrane and serves the purpose of rereducing the oxidized special-pair of the electron transfer chain (Figure 1).^{26,27} The four hemes are grouped into

pairs of low- and high-potential cofactors, and these pairs are arranged such that a chain of alternating low/high redox potentials is created through to the special-pair (i.e., low, high, low, high, SP; Figure 1).^{28,29} In this order, the individual hemes will be referred to here as H1, H2, H4, and H3, respectively (adopted from order of connection to the protein backbone). Previous studies regarding the factors responsible for controlling the hemes' in situ potentials have achieved accuracy to within ± 25 mV via electrostatic calculations, delineating the effects of charged residues in the vicinity of the heme, the protonation state of the heme propionates, the axial ligands of the heme-Fe, and the interheme redox couplings but including only marginally the effects of the hemes' varying conformations.³⁰

Since there are 15 crystal structures available from the PDB of the *B. viridis* reaction center, the question arises as to which one to select to perform the final part of our analysis? Our previous experience in this area suggests that standard quality metrics (e.g., resolutions, R-factors) for these large biomolecule crystal structures are not necessarily the decisive factor when one is interested solely with the detailed conformation of the cofactors.¹⁰ Instead therefore, we opted to perform a statistical analysis of the resolved conformations from all of the crystal structures and in so doing were able to uncover, and somewhat characterize, latent experimental biases which resulted in three sets of mean cofactor conformations (i.e., 12 heme structures) for our calculations.

To summarize, the focus of this paper is the proposal of a facile technique to predict and delineate the redox influence of macrocycle distortion in hemes and its application to further elucidate the role conformational control plays in the reaction center cytochrome subunit of *B. viridis*.

EXPERIMENTAL SECTION

Raw Data and NSD. The crystallographic atomic coordinates of the relevant H-NO_x and RC-CYT hemes were obtained from the PDB Ligand Expo³¹ and analyzed using the procedure of normal-coordinate structure decomposition (NSD)³² in which the macrocycle conformation is described by a linear decomposition into a basis composed of the macrocycle's internal normal-modes of vibration. This basis may consist of either the full set of 66 ($3N - 6$) *normal-coordinates* or any given subset. In their original formulation, Jentzen et al. termed the full set the *complete basis* and suggested two other useful bases: the *minimum* and *extended basis*.³² These reduced bases are composed of either the lowest-energy (min.) or the lowest- plus next-to-lowest-energy (ext.) normal-modes of each symmetry type. The utility of these reduced bases is that they yield a simplified analysis while their appropriateness is both allowed theoretically by the fact that the largest contributions to the observed conformations are expected to be distortions of relatively low energy and assessed practically by considering the root-mean-square deviation between the *simulated structure* (i.e., the conformation represented by the reduced basis) and the actual structure. Thus, NSD yields the magnitudes of each of the component normal-modes present in the chosen basis that contribute to the analyzed structure and provides a quantitative interpretation of the conformation. These data were used to determine the estimates of the RC-CYT heme conformations via a statistical analysis of the available crystal structures in a manner described in detail previously¹⁰ (see also below) and to construct the various cofactor models used for the calculations.

Theoretical Method. The model structures used as inputs for the density functional theory (DFT) calculations were selected so that the heme cofactor's structural parameters (i.e., substituent orientation, Fe-position, macrocycle conformation [including NSD reduced bases]) would be treated individually. The "diacid" model structures were formed by adding hydrogen atoms to the crystallographically resolved

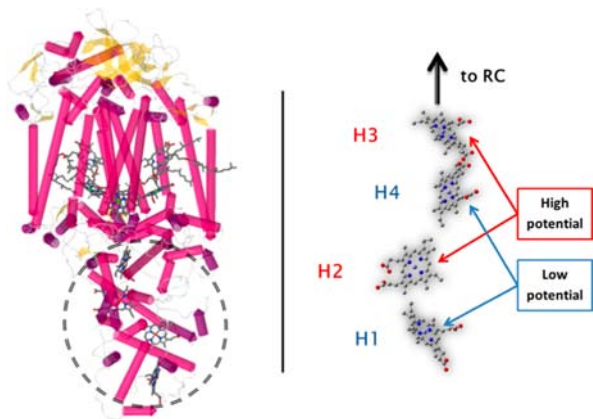


Figure 1. Illustration of the tetraheme cytochrome subunit in the reaction center of *B. viridis* (image adapted from the coordinates of PDB ID: 1PRC).

cofactor coordinates, adding the propionic acid proton to the oxygen with the longest C–O bond. The first Fe-porphin (FeP) model was also obtained directly from the crystal structure coordinates by replacing the macrocycle side-chains with hydrogen atoms. The “FeP-min, -ext, and -comp” models were generated by projecting the relevant weighted normal-deformations (minimum, extended, or complete, respectively) back onto the reference macrocycle in 3D-Cartesian space and by positioning the Fe-atom at the coordinate-system’s origin (since the reference macrocycle is centrosymmetric about this point) thereby providing a reduced model that accounts only for the macrocycle normal-mode distortions alone, eliminating any possible macrocycle conformation/Fe-position interaction.

The quantum calculations were performed with the Gaussian 09³³ package using the facilities of the Trinity Centre for High-Performance Computing. The Fe-atom Mulliken³⁴ and minimal basis set Mulliken^{35,36} atomic charges ($Q_{\text{Fe-Mullik}}$ and $Q_{\text{Fe-MBS}}$, respectively) of the heme models were obtained from single-point energy calculations using the B3LYP functional³⁷ and various basis sets. Natural atomic charges and orbital occupancies were obtained from Natural Population Analysis³⁸ using the NBO 3.1 implementation in Gaussian 09. In particular, we performed each calculation using the 3-21g,^{39,40} 6-31g*, 6-311g**,^{41–44} and 6-311+g**^{41–44} basis sets to roughly ascertain the parameters’ basis set dependency and so to find an appropriate balance between accuracy and expense. H-atom optimizations were not performed (to save on computational expense) as earlier trial computations (Supporting Information, Figure 1) indicated that they had no bearing upon the resultant Mulliken charges compared to the default hydrogen atom addition parameters used by the GaussView⁴⁵ software for SP²-carbons (i.e., $d(\text{C–H}) = 1.07 \text{ \AA}$ and $\angle(\text{R1–C–H}) = \angle(\text{R2–C–H}) = [360^\circ - \angle(\text{R1–C–R2})]/2$ such that the added hydrogen is coplanar with the SP² center and its other directly bonded atoms).

Statistical Analysis of Cofactor Conformations. Analysis of the conformations of the RC–CYT hemes began with agglomerative hierarchical clustering (AHC) of each cofactor’s minimum basis NSD to discover whether or not the crystal structure data were consistent with the hypothesis of distinct cofactor conformations. Thus, the AHC was performed on data matrices containing observations of the NSD minimum basis for each cofactor within the R statistical environment⁴⁶ using the Euclidean distance measure to build the dissimilarity matrix and Ward’s method for the agglomeration.

The method of AHC was ideal for this purpose because it provides information relating to the similarity of observations based on any number of numerical variables. In detail, observations are algorithmically grouped together (clustered) based on their mutual (dis-)similarity, calculated using a suitable distance metric; here, the Euclidean distance ($d_{ij} = \sqrt{[\sum(x_i - x_j)^2]}$). The decision as to how many clusters to select, between the extremes of one cluster containing all observations and as many clusters as there are observations, was achieved by consideration of the cluster dendrogram, which shows the interrelationships between possible clusters. For the agglomeration step, we used Ward’s method which can be considered to agglomerate with respect to reducing the information loss at each step. Therefore in chemical terms, since we clustered the NSD deformations of the cofactors, we obtained groups of cofactors that had similar resolved conformations.

To identify and isolate any systematic discrepancies between sets of structure determinations, the collected NSD data were then treated so that each PDB entry was considered as an individual observation and the minimum basis NSD deformations of its cofactors the observables. In detail, the data was formed into an $m \times n$ matrix where m is equal to the number of crystal structures included and n , the number of variables, equals the number of cofactors included (i.e., four hemes) multiplied by the number of NSD basis parameters used (e.g., B_{2u} of H1 is a distinct variable from B_{2u} of H2 and there is no categorical variable for cofactor identity). In the analyses of the experimental effects that followed, the 12 normal-coordinates of the minimum basis were used for each cofactor leading to a data set of 15 observations of 48 variables. Application of both AHC and principal components analysis (PCA) to this data matrix allowed the crystal structures to be

classified into groups exhibiting similar systematic errors (leaving only random fluctuations within each group) from which the mean conformations could be derived in the usual way.

Note that PCA, which here was used to complement AHC, is used to reduce the effective dimensionality of the data’s variable space by forming linear combinations of the original variables termed the principle components (PCs) which account for as much variance, with as few PCs, as possible (cf. AHC which combines *observations*). Thus, here the PCs represent distortions along vectors made up of combinations of the normal-modes from the NSD analysis of the *four* cofactors in each structure and hence illustrate the influence of the structure determination *classification* (from the AHC) upon the resolved conformations.

RESULTS AND DISCUSSION

Calibration of a Computational Procedure for Evaluating Heme Conformational Control. Initially, a number of computable parameters were tested to identify one which would correlate with the relative reduction potential shifts due to conformational control in the H-NOx WT, P115A, ISL and P115A/ISL complexes. The first attempt involved calculating standard estimates of the ionization potentials of the hemes in the form of HOMO (Koopmans’ theorem) and ΔDFT ($E_{\text{cation}} - E_{\text{neutral}}$) energies; however, in these experiments no simple correlation with the observed trend in reduction potentials was found. Next, recalling the electron deficiency that had been observed by Olea et al.²⁵ we thought it possible that this may be manifested in the Fe-atom partial atomic charges derived from atomic population analysis.

Thus, first the Fe-atom Mulliken atomic charges ($Q_{\text{Fe-Mullik}}$) were tested against the experimentally determined potentials (E_m ’s) of the H-NOx mutants where they provided, under certain conditions, strong, positive correlations. In particular, we found that $Q_{\text{Fe-Mullik}}$ from the singlet state B3LYP/3-21g wave functions correlated well with the H-NOx potentials (Supporting Information, Figure 2A) but that the corresponding triplet state calculations resulted in $Q_{\text{Fe-Mullik}}$ ’s that showed only slight correlation (Supporting Information, Figure 2B). Also, $Q_{\text{Fe-Mullik}}$ ’s obtained from any of the other basis-sets tested, in either state, provided poor correlations that often showed nonmonotonic relations. Even though the strong correlation of the singlet state $Q_{\text{Fe-Mullik}}$ with the H-NOx E_m ’s appeared to satisfy our requirements, the lack of a good correlation with the equivalent triplet state partial-charges was worrisome since this state represented the ground state of our models (affording lower total energies (Supporting Information, Tables 9–13) in accord with previous work on unligated Fe-porphins⁴⁷) and furthermore, the failure to reproduce the correlation with the larger, more appropriate basis sets could lead to doubts regarding our causal interpretation of the result. These problems necessitated further analysis and given the well-known numerical instability of Mulliken population analysis with respect to basis set size,⁴⁸ we investigated alternative approaches.

The first of these was chosen to circumvent the basis set dependency of the Mulliken analysis directly, while retaining the remainder of the formalism. The method, known as minimum basis set Mulliken analysis (MBS) proceeds by projecting the MO-LCAO coefficients of the original basis onto those of a minimal basis and only thereafter performing the standard Mulliken analysis on these new MOs.^{35,36} As hoped, the Fe-atom partial atomic charges obtained in this way ($Q_{\text{Fe-MBS}}$) provided remarkably improved correlations with the triplet state wave functions found using bases larger than 3-21g;

confirming that the failures there were due to the basis sensitivity of Mulliken analysis and suggesting that the 3-21g basis was insufficient to reasonably describe the triplet structure. However, a few anomalous results were present. Specifically, irregular drops of either one of the 1U56 cofactors occurred using the 6-31g* basis with the diacid and FeP-ext. models as well as with the 6-311g** result for the FeP model. Also, nonmonotonicity of $Q_{\text{Fe-MBS}}$ from the singlet calculations using the 6-31g* and 6-311g** bases was observed such that the former resulted in charges for the ISL (3NVR) cofactors that were less than those from ISL/P115A (3NVU), while the latter basis yielded $Q_{\text{Fe-MBS}}$ for ISL/P115A that were lower than the P115A (3EEE) structures (Supporting Information, Tables 2–4). On the other hand, progressively better correlations were obtained with increasing basis flexibility as may be expected for a truly causal, electronic relationship; gradual improvements observed for the triplet calculations and a discrete jump in agreement for the singlet state model with the 6-311g** basis so much so that their respective calibration curves are statistically identical. With this in mind, the anomalies cited above should not represent any serious problem for our purpose since we are concerned primarily with the ground state (triplet) of the FeP-comp. model (as this represents the best way to isolate fully the conformational influence) and are satisfied with the conclusion that the most flexible basis set employed here should be used to effect the most reliable results. Even so, for additional confirmation, we experimented with an entirely different form of population analysis, namely the Natural Population Analysis (NPA).³⁸

Surprisingly, the Fe-atom partial charges obtained via NPA ($Q_{\text{Fe-NPA}}$) exhibited an *inverse* correlation with the H-NOx E_m 's, this being in contrast to the previous $Q_{\text{Fe-MBS}}/E_m$ trends, which were consistent with the experimental results from the H-NOx mutants (*vide supra*). Closer inspection warranted, we found that this corresponded to an increase of both total valence and Rydberg Fe-atom natural orbital occupancies that overshadowed a decrease in the corresponding core orbital occupancies. Although we are currently unable to rationalize and explain this phenomenon, and can find no other report of such inverse proportionality between these two methods in the literature, the strong empirical relationship, lack of anomalies for the 1U56 cofactors, and reduced basis- and spin-state dependencies encouraged pursuit of NPA as a complementary approach, specifically using the Fe-core occupancy (CORE_{Fe}), not only because this parameter remained consistent with the previous findings and expectations, but also because it provided the best correlations (Supporting Information, Tables 30–32).

Turning now to the influence of the structural model used, the heme-diacid (not available for 6-311g**), FeP and FeP-comp. triplet models provided very similar results (Figure 2, bottom), regardless of basis, emphasized by linear relations with gradients, intercepts, and R^2 values within the ranges of 0.99–1.06; (–0.04)–0.00, and 0.98–1.00 for $Q_{\text{Fe-MBS}}$ (excluding the 1U56–B501 charge when outlying) and 0.89–1.07; (–1.22)–1.98, and 0.96–1.00 for CORE_{Fe} (all results), respectively. These high values of R^2 confirm beyond doubt that it is purely the induced macrocycle conformation which is the cause of the potential shifts in these H-NOx mutants and that a complex interaction between the macrocycle conformation and its side-chains, Fe-center, axial ligands, and/or protein environment is not involved. We can comment also that the same behavior holds true for all of the structural models in the singlet state using the 3-21g basis, but we did not perform the full set of

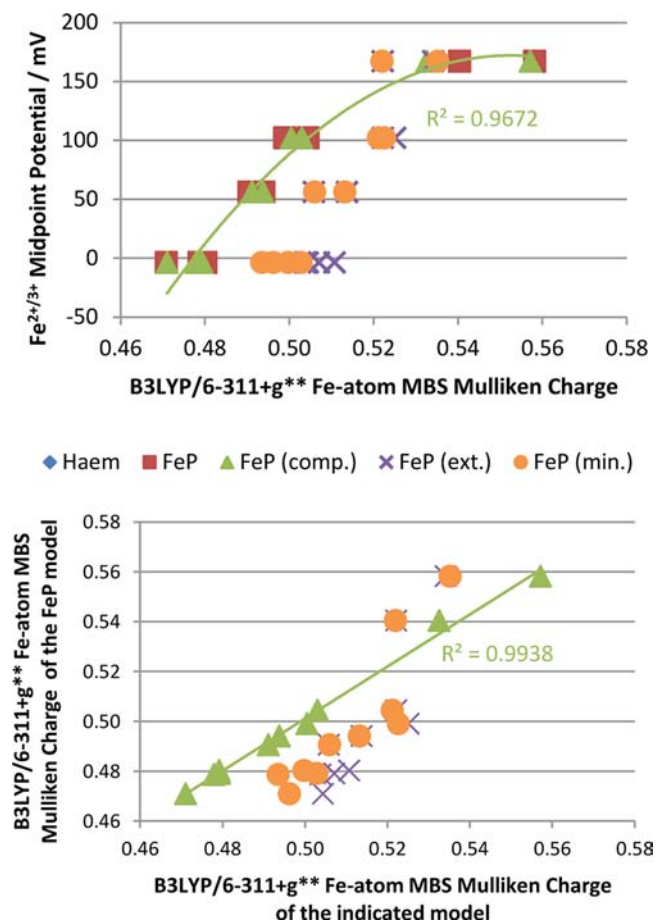


Figure 2. Plot of the measured $\text{Fe}^{2+/3+}$ midpoint potentials of the H-NOx mutants versus the calculated partial atomic charges of the heme-Fe ($Q_{\text{Fe-MBS}}$) from the various model structures in the singlet state (top) and correlation between $Q_{\text{Fe-MBS}}$ of the FeP model versus the other models of decreased complexity (bottom).

calculations for the remaining bases (only the FeP-comp. structures were assessed).

Additionally, the second order polynomial fits for these models' central-Fe charges and core populations as explanatory variables for the midpoint shifts resulted in correlation coefficients all greater than 0.93 for the former (with the same exclusions outlined above) and 0.95 for the latter implying their suitability for interpolating the intrinsic potential shifts brought about by conformational control here and in other systems.

With respect to the effect of the structural model, the oversimplified FeP-min and -ext. structures were only able to somewhat reproduce the relative experimental trends, especially with respect to the wild-type structure where the largest discrepancy, arising from heme 1U56 - B501, is the result of its resolved conformation, in which the minimum basis distortions are very much smaller than its counterpart in the asymmetric unit (Figure 3, note large error bars, and Supporting Information, Table 43). However, the reasonable degree of linearity found within the results from the mutant complexes (e.g., $R^2 = 0.90$ for the linear relation between H-NOx E_m and the FeP-min. CORE_{Fe} from the triplet calculations with the 6-311g**) suggests that knowledge of the reduced basis NSDs may allow extraction of trend information, in the limit of low total distortion and with caution. This could be advantageous in

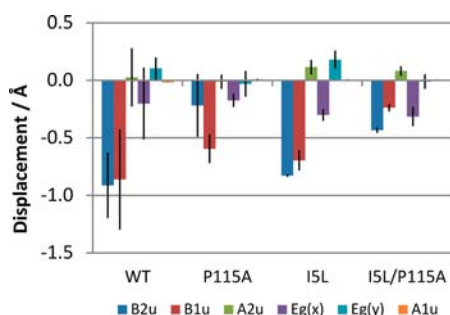


Figure 3. Mean out-of-plane minimum basis NSD of each heme from the H-NO_x crystal structures used in the calibration. Error bars indicate two standard errors; PDBs 1U56, 3NVR, and 3NVU, $n = 2$; 3EEE, $n = 4$ (hemis in asymmetric unit).

situations where resolutions are poor (since low energy distortions are often larger than their higher energy counterparts and therefore easier to resolve), although for this to be possible it is clear that further work regarding the precise sensitivity of the calculated parameters upon higher energy distortions is necessary before their application in quantitative work.

Another feature of the FeP-min and -ext. models is that the more planar mutant structures exhibit a systematically greater calculated partial charge at the heme-Fe. This may be either a consequence of the lack of higher-energy distortions that correlate with those of lower-energies of the same symmetry or else the result of a subtler aspect of the NSD process itself, specifically that the reference macrocycle used for the in-plane deformation decomposition is a Cu-porphine,³² which may mean that some higher-energy in-plane distortions are necessary to describe particular characteristic differences between this reference and an Fe-porphin. On the other hand, the systematically lower partial charges of the reduced basis models of the wild-type cofactors is most likely the result of the increasing dominance of the higher-energy distortion modes in affecting the molecular wave function and thus we suggest that it is the relationships between the distortions that is the cause of this behavior.

Derivation of Best Estimate(s) of Heme Conformations in *B. viridis* Cytochrome Subunit. The first task in elucidating the extent of conformational control in the RC-CYT subunit was to confirm that they possess distinct conformations with respect to one another. As previously shown,¹⁰ and discussed in the experimental section, this can be achieved by agglomerative hierarchical clustering (AHC) of their NSDs. In this case, the clustering of the cofactors' NSDs was predominantly dependent upon the cofactor's identity which shows that the crystallographic experiments supported the hypothesis that each cofactor adopted a unique conformation (Supporting Information, Figure 3). However, further consideration as to the composition of the clusters indicated that the H1 cofactors exhibited two distinct possible distortion patterns, a feature that was either related to two actual conformers or else to systematic differences between experiments (i.e., different systematic errors), in which the conformation of H1 is most affected. Since the previous experience has been that systematic differences can and do occur between multiple crystal structures of this type of macromolecule, which can be attributed to restraints during refinement,¹⁰ and because cluster measurement appeared heavily dependent on the structure authors (Supporting

Information, Table 1), we investigated the possibility of the latter via analysis of the "structure-as-observation" data-matrix.

The dendrogram and evolution of the within cluster sum of squares from the AHC of the structure-as-observation matrix suggests that there are 2–4 meaningful clusters, within which the structures show similar trends for the conformations of the cofactors and between, they exhibit systematic variations (Figure 4, top and Supporting Information, Figure 5).

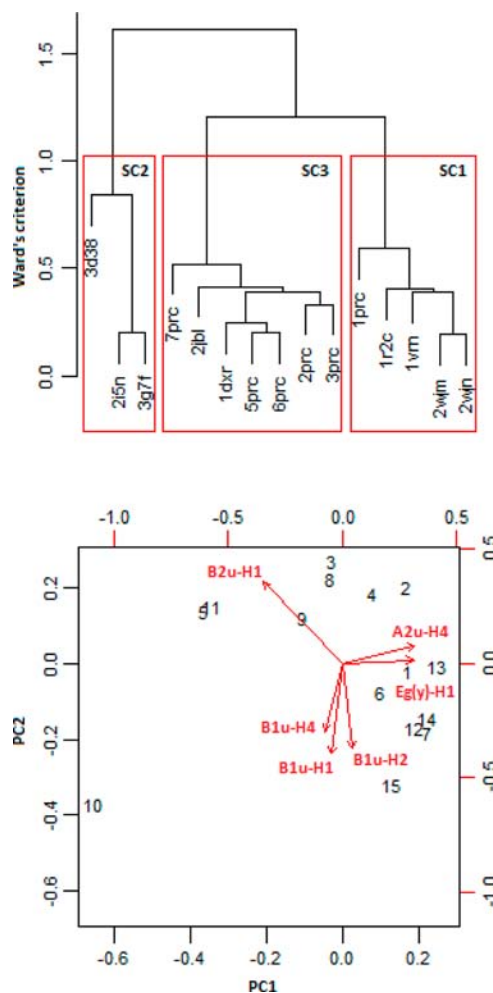


Figure 4. Dendrogram from the AHC of each PDB structures resolved minimum basis, out-of-plane NSDs of the four cofactors using the Euclidean metric and Ward's agglomeration (top; see Supporting Information, Table 1 for structure key). Biplot from the PCA of the PDB structures' resolved minimum basis out-of-plane conformations of the four cofactors on the first two PCs and the top 25% correlating variables (bottom).

Furthermore, the correlation biplot from the PCA analysis of the systematic variations (Figure 4, bottom and see Supporting Information, Figure 4 for scree-plot) shows that the greatest contributing variable to the systematic differences is the B_{2u} distortion of H1 and hence the bimodal conformation of H1 noted above is in fact the greatest discriminator between the structure classes. The next key variables are the B_{1u} distortions of the H1, H, and H4 cofactors, and it is these correlations that all but confirm that the differences between the structures are artificial since there is no known reason for the conformations of the cofactors to be coupled in this way. Also notable is the significant dependence of PC1 on the A_{2u} mode which becomes

increasingly apparent when the mean conformations of the clusters are considered (Figure 5; note relatively large A_{2u} distortion of SC2 cofactors and correlate with their positions in Figure 4 biplot [structures 5, 10 and 11]).

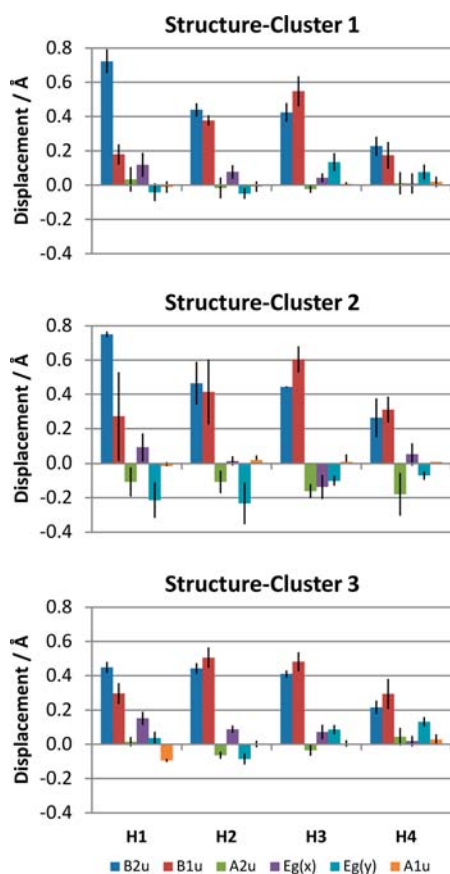


Figure 5. Mean out-of-plane minimum basis NSD of each heme cofactor from each cluster of crystal structures. Error bars indicate two standard errors. SC1 $n = 5$, SC2 $n = 3$, and SC3 $n = 7$.

On the basis of this information we proceeded with a three cluster solution giving rise to three sets of mean conformations (Figure 5) highlighting the particular conformations of each cofactor and also confirming that the two apparent conformers of the H1 cofactor are largely characterized by the extent of the saddling (B_{2u} mode) of the macrocycle. In addition to this we see that, on the whole, the minimum basis distortions of the cofactors indicated by the means of SC1 (structure-cluster 1) and SC2 are in some ways more similar than those of SC3 (in contrast to the relationship indicated by the cluster hierarchy; Figure 4, top). Specifically, the saddling of H1 in SC1 and -2 is relatively large, whereas in SC3 it is similar across H1–H3 and the relative amount of saddling to ruffling (B_{1u}) across H1–H3 is more consistent between SC1 and -2 compared to SC3. However, the main feature that differentiates the SC2 cluster is the high-degree of doming (A_{2u}) compared to structure sets SC1 and SC3. In SC3 also, the conformations of the cofactors are more similar across the hemes possibly indicating a greater influence of refinement restraints which could be responsible for the lesser nonplanarity of its conformation for H1 (Figure 5).

Conformational Control in the *B. viridis* RC Cytochrome Subunit. Having established both a quantitative empirical relationship between the FeP-comp. models' triplet

state B3LYP/6-311+g** Fe-atom MBS Mulliken atomic charges and the conformationally induced redox shifts, alongside the best estimate of the RC–CYT cofactors' conformations, we next sought to estimate the role of macrocycle mediated redox control in the RC–CYT.

Providing first a qualitative consideration of the particular structure-cluster results we see the SC1 structures' Fe-atom MBS Mulliken charges lie in the order $H1 < H2 \approx H3 \ll H4$ implying that naturally evolved conformational control contributes to the observed low-potential of the H1 cofactor, the $H2 > H1$ potential difference, is consistent with the similar potentials of the H2 and H3 cofactors and in some way works to increase the potential of the H4 cofactor. Alternatively, SC2 yields Q_{Fe-MBS} that vary so that $H1 \approx H2 < H3 \approx H4$ which corresponds with the fact that the H4/H3 low- and high-potential pair cofactors have systematically higher potentials than the corresponding H1/H2 pair. Finally, the SC3 conformations give Q_{Fe-MBS} ordered $H1 > H2 \ll H3 \approx H4$ which again corresponds with the observed larger potentials of the H4 and H3 pair but uniquely suggests that the conformational differences exerts influence to raise the H2 potential relative to H1. While these results show clear differences between the inferred conformational effect, an emergent trend is clear; it seems that conformational control operates to raise the potentials of the H3/H4 pair relative to their counterparts (or conversely, to lower those of the H2/H1 pair). Before discussing this further however, we consider now the quantitative estimations of the distortion/redox influence.

Noting that the RC–CYT Fe-atom MBS Mulliken charges (Figure 6) all fall within the range of interpolation from the H-NOx calibration (H-NOx FeP-comp: SC1, 0.489164–0.505313e; SC2, 0.483259–0.487204e; and SC3, 0.499779–0.514082e) (FeP-comp: $E_m \approx -30440 Q_{Fe}^2 + 33634 Q_{Fe} - 9118.6$), we obtained the “H-NOx potentials” (vide infra), allowing calculation of the relative potential shifts due to conformational control (Table 1).

In terms of a formal interpretation, if one considers that the reduction potential of a heme in a protein complex arises from a combination of perturbations effected by the environment relative to a free heme (reference) in solution, then the potential may be written as a sum of the reference potential and the perturbation as,

$$E_m^{\text{complex}} = E_m^{\text{solution}} + \Delta E_m^{\text{perturbation}}$$

where the last term is a sum of the contributions from all environmental considerations such as H-bonding, electrostatics, axial-ligands (if different from the reference), solvent accessibility and conformational control. In our case, since we are interested solely in delineating the effect of conformational control we may write this as,

$$E_m^{\text{H-NOx}} = E_m^{\text{solution}} + \Delta E_m^{\text{H-NOx(environment)}} + \Delta E_m^{\text{conformation}}$$

then, since the H-NOx series of complexes investigated varied solely in the last term, taking the difference of any two of their potentials yields exclusively the change in this component,

$$\Delta E_m^{\text{H-NOx}} = \Delta(\Delta E_m^{\text{conformation}})$$

Consequently, taking the difference of any two interpolated “H-NOx potentials” (the potential that the H-NOx complex would exhibit if the heme within adopted the conformation of

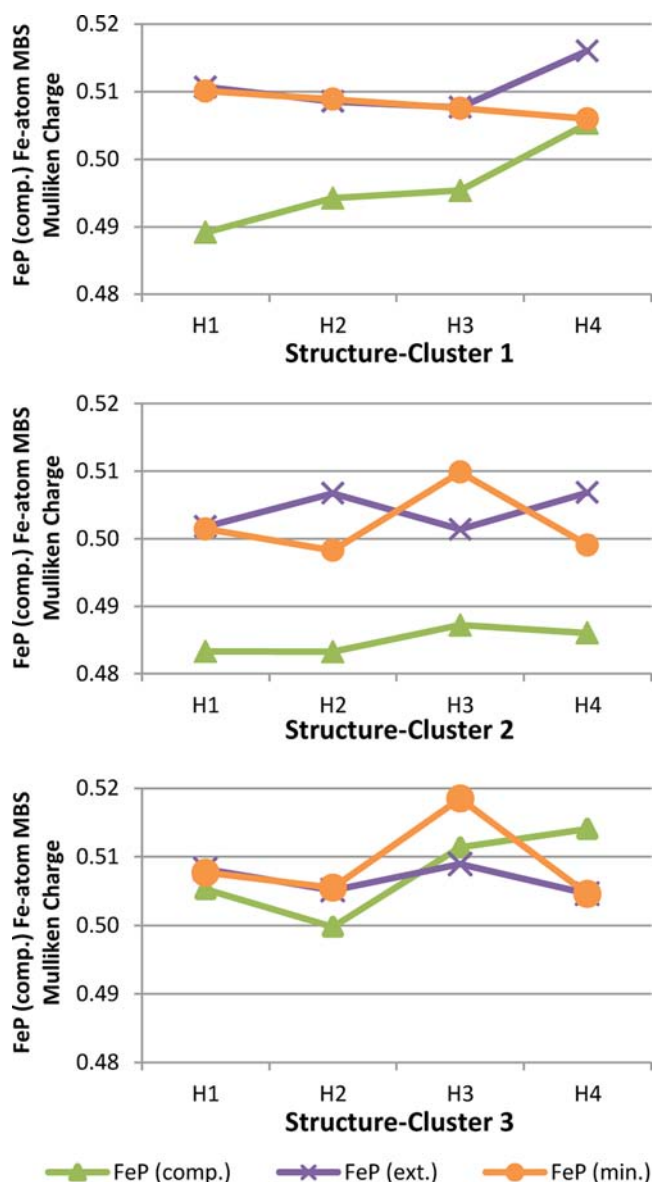


Figure 6. Fe-atom MBS Mulliken partial atomic charges ($Q_{\text{Fe-MBS}}$) calculated from mean FeP-comp., -ext., and -min models of the three structure-cluster *B. viridis* RC-CYT hemes mean conformations in the triplet state with the B3LYP/6-311+g** method.

interest), yields the potential difference effected by their conformational difference.

The one possible caveat to this approach is that the extension of the H-NO_x relationship to other proteins is dependent on whether or not the magnitude of the intrinsic potential shift brought about by macrocycle distortion is sensitive to the specific environment of the cofactor. Since there is no suggestion in the literature to the contrary we proceed to investigate the impact of conformational control on the *B. viridis* hemes under the assumption that there is no such effect, although it must be noted that it is certainly possible that there are such differences.

The data in Table 1 show the experimental and most recent, state-of-the-art, theoretically calculated cofactor potential shifts together with the estimated influence of conformational control obtained from our highest level calculation (B3LYP/6-311+g**). The interpretation of the entries in the middle of

the nonexperimental data correspond to the percentage of the difference accounted for by the quoted method, for example, Voigt and Knapp's method accounted for 48% (36 mV) of the H1–H4 difference while our method suggests that 72% (54 mV) of the difference is due to conformational control.

In most cases, the calculated perturbation of conformational control affects a change in potential that acts in concert with the other modulatory methods of the binding-site to increase the potential difference between cofactors (i.e., has the same sign as the experimental difference), except for H4 relative to both H2 and H3. Indeed it is notable that the H4–H2 difference is the only one which Voigt and Knapp's method overestimated, while that of H4–H3 is the only one that was not underestimated (the near exact agreement of their value for this difference is due in fact to a systematic error of around –30 mV in both the H3 and H4 absolute potentials). Furthermore, the two largest potential differences due to conformational control as inferred from any one of the three sets of mean conformations are found to involve the H3 or H4 potentials with those of H2 or H1 (respectively) such that the potentials of the former are raised relative to the latter (Table 1).

It is convenient to assess the quantitative implications of our work in the context of improving the current theoretical understanding of the factors affecting the heme potentials by combining the Voigt and Knapp estimates of the interheme potential differences with any one of our estimates of the influence of conformational control. This should be deemed acceptable under the assumption that those previous theoretical estimates were precisely lacking this effect and because our isolation of it is total. Importantly, doing so provides significantly improved experimental agreement (RMSDs = 27 mV for Voigt and Knapp, and 19 mV, 17 mV, and 20 mV after including the estimated conformational effect from mean conformations SC1, SC2, and SC3, respectively). Furthermore, considering the individual corrections, it is clear that the SC1 structures' derived shifts may well provide an even greater improvement to the absolute potentials than is implied by the reduction of the RMSD experimental agreement of the interheme relative differences because these results break the effect of Voigt and Knapp's systematic error for the H3 and H4 cofactors, if we were able to determine these soundly.

While we have already suggested that the H1 conformation of SC3 may be less reliable from the structure-determination point of view, a pragmatic view of these results also suggests that this may be an erroneous result. This point is taken simply from the observed experimental disagreement of the predicted relative cofactor potential differences, the H1–H2 difference, which was already underestimated, is even more worse off with SC3's contribution, and there is no systematic error in the theoretical potentials for these as there was with the H3–H4 cofactors (see above).

Conformational Origin of Haem Redox Modulation. A key feature that we have not yet discussed is that in the *B. viridis* cytochrome subunit, it is the cofactor with the lowest total nonplanar distortion (H4, Figures 5 and 6) that exhibits a consistently high relative partial charge and that the cofactor with the greatest distortion exhibits one of the lowest charges (H1), which is in stark contrast to the situation in the H-NO_x complex. Thus, it appears that the redox influence of the cofactor conformations is inverted between the two complexes. To begin to explain the origin of this phenomenon, we are required to investigate the correlations between the macrocycle modes of distortion and the calculated population parameters.

Table 1. Conformational Effect on the *B. viridis* Cytochrome Interheme Potential Differences

	cofactor potential differences/mV ^a				expt. correlation ^b				expt. error of Voigt and Knapp with conformational shift / mV ^c				change in absolute expt. error/mV ^d			
	H1	H2	H3	H4	H1	H2	H3	H4	H1	H2	H3	H4	H1	H2	H3	H4
expt. average ^{28,29}	H1	0	365	435	75											
	H2	-365	0	70	-290											
	H3	-435	-70	0	-360											
	H4	-75	290	360	0											
Voigt and Knapp ³⁰	H1	0	348	395	36	0.95	0.91	0.48		-17	-40	-39				
	H2	-348	0	47	-312		0.67	1.08				-23	-22			
	H3	-395	-47	0	-359			1.00						1		
	H4	-36	312	359	0											
SC1	H1	0	19	23	54	0.05	0.05	0.72		2	-17	15		-15	-23	-24
	H2	-19	0	4	36		0.06	-0.12				-19	14		-4	-8
	H3	-23	-4	0	32			-0.09					33			32
	H4	-54	-36	-32	0											
SC2	H1	0	0	16	11	0.00	0.04	0.15		-17	-24	-28		0	-16	-11
	H2	0	0	16	11		0.23	-0.04			-7	-11			-16	-11
	H3	-16	-16	0	-5			0.01					-4			3
	H4	-11	-11	5	0											
SC3	H1	0	-17	16	23	-0.05	0.04	0.31		-34	-24	-16		17	-16	-23
	H2	17	0	33	40		0.47	-0.14				10	18		-13	-4
	H3	-16	-33	0	7			-0.02					8			7
	H4	-23	-40	-7	0											

^aAbsolute interheme potential differences [$D_{ij} = H_j - H_i$]. The entries for SC1-3 are derived from the differences of $E_m(\text{H-NOx})$ found by application of the H-NOx calibration to QFe-MBS obtained from the triplet state B3LYP/6-311+g** wavefunctions of the FeP-comp. structures from the respective structure-cluster. ^bInterheme potential differences relative to experiment [$D_{ij} = (H_j - H_i)_{\text{calc}} / (H_j - H_i)_{\text{expt}}$]. ^cThe entries for SC1-3 indicate the experimental error obtained after the summation of the Voigt and Knapp potential differences with the difference imposed by the cofactors' unique conformations. ^dThe difference between the combination model interheme potential absolute errors (e.g., Voigt and Knapp with added SC1 shifts) with the Voigt and Knapp error alone.

The following discussion relates to our preliminary results only as, in general, the derivation of a logical relationship between heme conformation and electronic properties is a complicated endeavor and indeed one of our long-term goals.

Combining the H-NOx and cytochrome data and regressing the heme-Fe MBS Mulliken charges and NPA core populations against the individual NSD parameters revealed one candidate above all others as the main indicator of the electronic population at the metal center, namely, the A_{1g} or *breathing* mode. The extent of this distortion provided statistically significant correlation coefficients of 0.87 and 0.94 with the minimum basis cofactor projections and the corresponding $Q_{\text{Fe-MBS}}$ and CORE_{Fe} values and, 0.78 and 0.83 for the complete basis projections (observed macrocycle conformation, centered Fe) and corresponding populations. Furthermore, because this normal-mode represents most closely the actual macrocycle core size, and thus the Fe-N bond lengths, this behavior is perfectly understandable. We must highlight here that this result does not render the nonplanar macrocycle distortions as superfluous or secondary next to the in-plane conformation, as attempted by the outmoded concept of In-plane Nuclear Rearrangement, alluded to in the introduction. Rather, multicollinearities are present between the various normal-coordinates that suggest that the A_{1g} distortion is *determined* by the nonplanar distortions and thus provides a conduit with which the nonplanar conformation exerts the real influence. Indeed, this structural relationship has been known for many years²² and is supported by our own semiempirical calculations that find nonzero minima along the A_{1g} coordinate for arbitrarily imposed nonplanar distortions upon a previously optimized structure.⁴⁹

However, this analysis provides only explicit investigation of the global situation, that is, the source of conformationally induced potential shifts over a range of 171 mV and two distinct complexes (for one of which we had three sets of possible, systematically different structure determinations) while our maximum estimated effect of natural conformational control in the cytochrome was only 54 mV. Also, a perusal of the in-plane distortions of the *B. viridis* hemes (Supporting Information, Figure 9 and Table 28) suggested that while some of the variation appeared to correspond with the A_{1g} coordinate (in particular, the systematic lowering of the SC2 charges), this was by no means a conclusive resolution. Therefore, although at the expense of statistical sample size, to assess the situation in more detail we assessed the NSD/population parameter relations arising from meaningful subsets directly. Specifically, we additionally regressed subsets of the data composed from the H-NOx structures, the H-NOx mutants only (105 mV range), the H-NOx P115A and ISL/P115A mutants (60 mV range), the *B. viridis* mean conformations, and the individual structure-clusters of the latter.

Not unexpectedly, all but the largest of these subsets were too small to produce any *strictly* statistically significant correlations after alphas were adjusted for multiple comparisons. On the other hand, the results do suggest that the full set of A_{1g} modes may contribute to a considerable portion of the within group population variations. Nevertheless, even if these correlated in-plane distortions do provide the connection between the observed effects in each complex, it would then suggest that the nonplanarity induced contraction is reversed for the case of H4 which exhibits a *contracted* macrocycle even though it is the most planar.

There is however, a potential explanation for some of these observations. The first step is to understand that most likely it is the *ruffle* distortion that results in the greatest core contraction, as it is known to do so for Ni-porphyrins,²² and on this basis we can somewhat account for the H1–H3 Fe populations. Next, having only to account for the high-partial charge of H4 we consider that the bis-HIS coordination of this heme that effects a large drop in its reduction potential and a corresponding increased Fe atom electron density it is possible then that the macrocycle contracts to stabilize this extra density.

However, it may have to suffice to say that it is the particular conformation that determines the metal population and the consequent conformational contribution to the redox potential although it appears clear that the satisfactory experimental agreement afforded by our method implies that it is fully capable of accounting for this fact.

CONCLUSIONS

By applying chemical intuition in an attempt to obtain an experimentally calibrated computational procedure with which to predict and delineate the influence of protein-induced macrocycle distortion upon heme reduction potentials, a strong correlation between heme-Fe MBS Mulliken atomic charges obtained using B3LYP wave functions with minimal- to triple- ζ , doubly polarized augmented basis sets and the redox potentials of intact complexes could be established, in the circumstance that the heme conformation was the only substantially varying property. This relationship will assist future research in the realm of naturally occurring conformational control and with further development may also prove useful for the design and tuning of heme enzymes where conformational change from residue mutations could be predicted using standard geometry optimizations and, from the resultant cofactor conformation, the mutation's consequent physicochemical effect which could potentially reduce the cost and effort required to engineer proteins with desired redox properties.

Using this relationship together with the derivation of the best currently available estimates of the conformations' of the heme cofactors in the reaction center tetraheme cytochrome subunit of *B. viridis*, it was found that conformational control may account for up to 70% (54 mV) of a particular potential difference and correlates with the greater potentials of each heme in the pair proximal to the special-pair with their respective distal counterparts. The estimated influence upon the reduction potentials of H1–H3 appears to work concertedly with other protein influences to enhance the differences between them, while for H4 it significantly reduces effects of bis-HIS coordination^{26,27} and the partial ionization of its propionates.³⁰ This shows that explicit consideration of the conformational contribution to heme reduction potential modulation *in situ* may provide a missing link with respect to understanding heme potential variability in general.

ASSOCIATED CONTENT

Supporting Information

Additional figures and tables that are referenced in text: comparison of heme-Fe Mulliken atomic charges obtained with and without peripheral H-atom optimization, heme-Fe Mulliken charges from triplet calculations, cluster hierarchy and composition from AHC of cofactor NSDs from all PDB entries, scree-plots from statistical analyses, PDB entry structure authorship, resolutions, references and key for Figure 4, multivariate analysis of heme-Fe Mulliken charges obtained

from individual cofactor coordinates. Tabulated data: all data-values presented in charts, DFT-SCF energies, heavy-atom coordinates for models of reduced complexity, all cofactor minimum basis NSDs. Complete author list for reference 33. This material is available free of charge via the Internet at <http://pubs.acs.org>.

AUTHOR INFORMATION

Corresponding Author

*E-mail: sengem@tcd.ie.

Notes

The authors declare no competing financial interest.

ACKNOWLEDGMENTS

This work was supported by Science Foundation Ireland (SFI P.I. 09/IN.1/B2650). All calculations were performed on the Lonsdale cluster maintained by the Trinity Centre for High Performance Computing. This cluster was funded through grants from Science Foundation Ireland.

ABBREVIATIONS

AHC, agglomerative hierarchical clustering; H-NO_x, heme-NO and -O₂ binding domain; NSD, Normal-coordinate structural decomposition; PCA, principal components analysis; PDB, Protein Data Bank; RC-CYT, reaction center cytochrome subunit; SC(1–3), structure-clusters 1–3; SHE, standard hydrogen electrode

REFERENCES

- (1) Chapman, S. K.; Daff, S.; Munro, A. W. Heme: The most versatile redox centre in biology? In *Structure and Bonding* (Berlin); Hill, H., Sadler, P. J., Thomson, A., Eds.; Springer: Berlin, Germany, 1997, Vol. 88, pp 39–70.
- (2) Poulos, T. L. *Nat. Prod. Rep.* **2007**, *24*, 504–510.
- (3) Bertini, I.; Cavallaro, G.; Rosato, A. *Chem. Rev.* **2006**, *106*, 90–115.
- (4) Reedy, C. J.; Gibney, B. R. *Chem. Rev.* **2004**, *104*, 617–650.
- (5) Rodgers, K. R. *Curr. Opin. Chem. Biol.* **1999**, *3*, 158–167.
- (6) Breton, J.; Martin, J. -L.; Migus, A.; Antonetti, A.; Orszag, A. *Proc. Natl. Acad. Sci. U.S.A.* **1986**, *83*, 5121–5125.
- (7) Reedy, C. J.; Elvekrog, M. M.; Gibney, B. R. *Nucleic Acids Res.* **2008**, *36*, D307–13.
- (8) Zheng, Z.; Gunner, M. R. *Proteins* **2009**, *75*, 719–734.
- (9) Allen, J. P.; Williams, J. C. The Influence of Protein Interactions on the Properties of the Bacteriochlorophyll Dimer in Reaction Centers. In *Advances in Photosynthesis and Respiration*; Grimm, B., Porra, R. J., Rüdiger, W., Scheer, H., Eds.; Springer: Dordrecht, The Netherlands, 2006; Vol. 25, pp 283–295.
- (10) MacGowan, S. A.; Senge, M. O. *Chem. Commun.* **2011**, *47*, 11621–11623.
- (11) Senge, M. O. Highly Substituted Porphyrins. In *The Porphyrin Handbook*; Smith, K. M., Kadish, K. M., Guillard, R., Eds.; Academic Press: San Diego, CA, 2000; Vol. 1, pp 239–347.
- (12) Senge, M. O. *Chem. Commun.* **2006**, 243–256.
- (13) Scheidt, W. R.; Reed, C. A. *Chem. Rev.* **1981**, *81*, 543–555.
- (14) Kratky, C.; Waditschatka, R.; Angst, C.; Johansen, J. E.; Plaquevent, J. C.; Schreiber, J.; Eschenmoser, A. *Helv. Chim. Acta* **1985**, *68*, 1312–1338.
- (15) Hobbs, J. D.; Shelnut, J. A. *J. Protein Chem.* **1995**, *14*, 19–25.
- (16) Jentzen, W.; Ma, J. G.; Shelnut, J. A. *Biophys. J.* **1998**, *74*, 753–763.
- (17) Senge, M. O. *J. Photochem. Photobiol. B* **1992**, *16*, 3–36.
- (18) Fajer, J. *Isr. J. Chem.* **1992**, *32*, 363–518.
- (19) Röder, B.; Büchner, M.; Rückmann, I.; Senge, M. O. *Photochem. Photobiol. Sci.* **2010**, *9*, 1152–1158.

- (20) Senge, M. O.; Renner, M. W.; Kalisch, W. W.; Fajer, J. *Dalton Trans.* **2000**, 381–385.
- (21) Ryeng, H.; Ghosh, A. *J. Am. Chem. Soc.* **2002**, *124*, 8099–8103.
- (22) Haddad, R. E.; Gazeau, S.; Pecaut, J.; Marchon, J. C.; Medforth, C. J.; Shelnut, J. A. *J. Am. Chem. Soc.* **2003**, *125*, 1253–1268.
- (23) DiMugno, S. G.; Wertsching, A. K.; Ross, C. R. *J. Am. Chem. Soc.* **1995**, *117*, 8279–80.
- (24) Wertsching, A. K.; Koch, A. S.; DiMugno, S. G. *J. Am. Chem. Soc.* **2001**, *123*, 3932–3939.
- (25) Olea, C., Jr.; Kuriyan, J.; Marletta, M. A. *J. Am. Chem. Soc.* **2010**, *132*, 12794–12795.
- (26) Deisenhofer, J.; Epp, O.; Miki, K.; Huber, R.; Michel, H. *Nature* **1985**, *318*, 618–624.
- (27) Deisenhofer, J.; Epp, O.; Miki, K.; Huber, R.; Michel, H. *J. Mol. Biol.* **1984**, *180*, 385–398.
- (28) Dracheva, S. M.; Drachev, L. A.; Konstantinov, A. A.; Semenov, A.; Skulachev, V. P.; Arutjunjan, A. M.; Shuvalov, V. A.; Zaberezhnaya, S. M. *FEBS J.* **1988**, *171*, 253–264.
- (29) Fritsch, G.; Buchanan, S.; Michel, H. *Acta Biochim. Biophys.* **1989**, *977*, 157–162.
- (30) Voigt, P.; Knapp, E. W. *J. Biol. Chem.* **2003**, *278*, 51993–52001.
- (31) Feng, Z.; Chen, L.; Maddula, H.; Akcan, O.; Oughtred, R.; Berman, H. M.; Westbrook, J. *Bioinformatics* **2004**, *20*, 2153–2155.
- (32) Jentzen, W.; Song, X. Z.; Shelnut, J. A. *J. Phys. Chem. B* **1997**, *101*, 1684–1699.
- (33) Frisch, M. J. et al. *Gaussian 09*, Revision A. 02; Gaussian, Inc.: Wallingford, CT, 2009.
- (34) Mulliken, R. S. *J. Chem. Phys.* **1955**, *23*, 1833–1840.
- (35) Montgomery, J. A., Jr.; Frisch, M. J.; Ochterski, J. W.; Petersson, G. A. *J. Chem. Phys.* **2000**, *112*, 6532–6542.
- (36) Montgomery, J. A., Jr.; Frisch, M. J.; Ochterski, J. W.; Petersson, G. A. *J. Chem. Phys.* **1999**, *110*, 2822–2827.
- (37) Becke, A. D. *J. Chem. Phys.* **1993**, *98*, 5648–5652.
- (38) Reed, A. E.; Weinstock, R. B.; Weinhold, F. *J. Chem. Phys.* **1985**, *83*, 735–746.
- (39) Binkley, J. S.; Pople, J. A.; Hehre, W. J. *J. Am. Chem. Soc.* **1980**, *102*, 939–947.
- (40) Dobbs, K. D.; Hehre, W. J. *J. Comput. Chem.* **1987**, *8*, 861–879.
- (41) Raghavachari, K.; Binkley, J. S.; Seeger, R.; Pople, J. A. *J. Chem. Phys.* **1980**, *72*, 650–654.
- (42) Wachters, A. J. H. *J. Chem. Phys.* **1970**, *52*, 1033.
- (43) Hay, P. J. *J. Chem. Phys.* **1977**, *66*, 4377–4384.
- (44) Raghavachari, K.; Trucks, G. W. *J. Chem. Phys.* **1989**, *91*, 1062–1065.
- (45) Dennington, R.; Keith, T.; Millam, J. *GaussView*, Version 5; Semichem Inc.: Shawnee Mission, KS, 2009.
- (46) R Development Core Team *R: A language and environment for statistical computing*; R Foundation for Statistical Computing, Vienna, Austria, 2010.
- (47) Rovira, C.; Kunc, K.; Hutter, J.; Ballone, P.; Parrinello, M. *J. Phys. Chem. A* **1997**, *101*, 8914–8925.
- (48) Liu, W.; Li, L. *Theor. Chem. Acc.* **1997**, *95*, 81–95.
- (49) MacGowan, S. A.; Senge, M. O. unpublished results.